






RESEARCH PAPER

# Magneto-hydrodynamic mixed convection chemically rotating and radiating 3D hybrid nanofluid flow through porous media over a stretched surface

Katikala N. V. Ch. Bhargava <sup>1,†</sup>, Shaik Mohammed Ibrahim <sup>1,\*‡</sup> and Raghunath Kodi <sup>2,‡</sup>

<sup>1</sup>Department of Mathematics, Koneru Lakshmaiah Education Foundation, Green Fields, Vaddeswaram, Vijayawada-522302, Andhra Pradesh, India, <sup>2</sup>Department of Humanities and Sciences, St. Johns College of Engineering and Technology, Yemmiganur, Kurnool Dist, A.P 518360, India

\*Corresponding Author

†bhargavahcu@gmail.com (Katikala N. V. Ch. Bhargava); ibrahimsvu@gmail.com (Shaik Mohammed Ibrahim); kraghunath25@gmail.com (Raghunath Kodi)

## Abstract

This study presents a comprehensive 3D analysis of hybrid  $Fe_3O_4/Al_2O_3$  nanofluid flow over a stretched plate, incorporating the effects of buoyancy, Hall current, rotation, nonlinear thermal radiation, and Joule heating. A key novelty of the work lies in extending previous models by introducing mixed convection flow and a concentration equation, alongside thermophoresis and Brownian motion, offering a deeper understanding of hybrid nanofluid behavior in complex thermal environments. The governing partial differential equations are transformed into nonlinear ordinary differential equations using similarity transformations and solved numerically via the shooting method. These findings have critical implications for optimizing heat exchangers, cooling systems, and chemical reactors, where efficient thermal management is essential. The study's integration of multiple physical phenomena highlights its novelty and contributes valuable insights to the field of computational fluid dynamics and industrial applications. It is observed that increased buoyancy enhances the primary fluid velocity, but reduces the secondary velocity. This results in lower temperature and concentration profiles, indicating that buoyancy significantly affects the fluid's flow and thermal behavior.

**Keywords:** Stretching surface; chemical reaction; hybrid nanofluids; Hall current; boundary layer

**AMS 2020 Classification:** 74A15; 74A50; 76A05; 35Q30

## 1 Introduction

This study has the potential for wide-ranging practical applications, particularly in industries where efficient heat and mass transfer solutions are critical. Hybrid nanofluids, with their en-

hanced thermal properties, can significantly improve the performance of industrial heat exchangers. In power plants, refrigeration systems, and chemical industries, where heat management plays a key role in operational efficiency, hybrid nanofluids allow for faster and more uniform heat dissipation, leading to improved system performance and energy savings. Similarly, in cooling systems for electronics, such as in data centers, high-performance processors, and electronic devices, hybrid nanofluids can provide a highly effective thermal management solution, preventing overheating and extending the lifespan of electronic components. The study is also relevant to energy systems such as solar thermal systems and nuclear reactors, where precise control over heat transfer is essential for optimizing energy conversion and ensuring safety. The integration of magnetic fields and mixed convection flows in the analysis helps tailor heat transfer processes, making them more efficient in energy-intensive environments. Moreover, in chemical reactors, the incorporation of chemical reactions in the nanofluid model supports more accurate temperature and concentration control, ensuring that reactions proceed at optimal rates. This has practical implications for industries such as petrochemicals and pharmaceuticals, where precise thermal management can lead to higher yields and more efficient processes. Khan et al. [1] have applied mathematical modelling and heat transport investigation in hybrid nanofluids under the impact of thermal radiation. Adnan et al. [2] have studied the numerical investigation of heat transport in the nanofluids under the impact of magnetic fields and applications from industrial zones. Hakeem et al. [3] have discussed MHD Boundary Layer Flow over a Stretching Sheet: A New Stochastic Method. Kumar et al. [4] have expressed a heat transfer study for the flow of non-Newtonian nanofluid past a Riga plate with variable thickness. Fayz-Al-Asad et al. [5] have reviewed the influence of Fin Length on Magneto-Combined Convection Heat Transfer Performance in a Lid-Driven Wavy Cavity. Hossain et al. [6] have discussed a Numerical Study of the Effect of a Heated Cylinder on Natural Convection in a Square Cavity in the Presence of a Magnetic Field. Raghunath et al. [7] have studied the thermodynamic and buoyancy force effects of Cu and  $TiO_2$  nanoparticles in engine oil flow over an inclined permeable surface. Zhang et al. [8] have analyzed 3D-MHD mixed convection in a Darcy-Forchheimer Maxwell fluid: Thermo diffusion, diffusion-thermo effects, and activation energy influence.

The amalgamation of nano-sized particles such as carbon, copper, titanium, and their oxides in a conventional fluid is called nanofluid. Choi [9] pioneered the enhancement of thermal conductivity in fluids like oil, ethylene glycol, and water by adding nanoparticles, leading to applications in engine cooling, refrigerators, chillers, fuel cells, and microelectronics. Nanofluids also have medical applications, such as safer surgeries and cancer therapy. Ashorynejad et al. [10] found that magnetic fields increase wall shear stress in nanofluids, while Omar et al. [11] showed that higher nanoparticle concentrations boost heat flux and drag force. Mabood et al. [12] noted decreased heat and mass transfer with larger Lewis numbers and Brownian motion. Mabood et al. [13] studied unsteady nanoliquid flow on heated plates. Khan et al. [14] examined Powell-Eyring nanofluid flow, incorporating Brownian motion and thermophoretic effects, which was later extended by investigating dipole influence on the thermally radiative flow of Williamson nanofluids [15]. Ahmad et al. [16] explored nanofluid flow over a Riga surface, highlighting electromagnetic control of flow behavior.

The insights into thermophoresis, Brownian motion, and joule heating in this study offer valuable contributions to the aerospace and automotive industries. In these sectors, lightweight, high-efficiency cooling solutions are necessary for engines, exhaust systems, and avionics, where managing heat effectively is crucial for performance and safety. The ability of hybrid nanofluids to enhance thermal management in such applications underscores their potential to revolutionize heat transfer technologies across diverse industrial sectors. Shah et al. [17] have studied Brownian motion and thermophoretic diffusion effects on the dynamics of MHD upper convected

Maxwell nanofluid flow past a vertical surface. Shah et al. [18] have possessed modeling of bioconvective flow existing with tiny particles and quartic autocatalysis reaction across the stratified upper horizontal surface of a paraboloid of revolution. Oreyeni et al. [19] have discussed the thermal performance of radiative magnetohydrodynamic Oldroyd-B hybrid nanofluid with Cattaneo–Christov heat flux model: Solar-powered ship application. Fayz-Al-Asad et al. [20] have reviewed the analytic simulation of the MHD boundary layer flow of a chemically reacting upper-convected Maxwell fluid past a vertical surface subjected to double stratifications with variable properties.

In rotating machinery like turbines, pumps, and centrifuges, the analysis of rotation effects is critical because these machines generate significant heat during operation. The findings of this study could help improve the cooling systems used in such machinery, ensuring smooth operation and preventing overheating. Additionally, in biomedical applications, hybrid nanofluids have potential uses in hyperthermia treatments for cancer, where precise control over heat delivery is required to target tumor cells without damaging surrounding tissues. Dhananjay et al. [21] have studied the impact of rotation on the onset of cellular convective movement in a Casson fluid-saturated permeable layer with temperature-dependent thermal conductivity and viscosity deviations. Sunitha et al. [22] have studied Unsteady MHD rotating mixed convective flow through an infinite vertical plate subject to Joule heating, thermal radiation, Hall current, and radiation absorption. Hari Babu et al. [23] have reviewed Heat and Mass Transfer on Unsteady MHD Chemically Reacting Rotating Flow of Jeffrey Fluid Past and Inclined Plates under the Impact of Hall Current, Diffusion Thermo, and Radiation Absorption. Raghunath et al. [24] have possessed the Hall current and thermal radiation effects of 3D rotating hybrid nanofluid reactive flow via stretched plate with internal heat absorption. Raju et al. [25] have expressed Chemical Radiation and Soret Effects on Unsteady MHD Convective Flow of Jeffrey Nanofluid Past an Inclined Semi-Infinite Vertical Permeable Moving Plate. Sridevi et al. [26] have reviewed an investigation into the impact of thermal radiation and chemical reactions on the flow through porous media of a Casson hybrid nanofluid including unstable mixed convection with stretched sheet in the presence of thermophoresis and Brownian motion.

Magnetohydrodynamics (MHD) explores the behavior of electrically conducting fluids, like plasmas and liquid metals, in the presence of magnetic fields, which influence the fluid's motion and create complex interactions. MHD has significant applications across various fields. In industrial cooling systems, particularly for nuclear reactors, MHD helps control the flow of liquid metal coolants, enhancing heat transfer. In astrophysics and geophysics, MHD explains phenomena like solar flares and planetary magnetic fields. It's also critical in fusion reactors for controlling plasma in magnetic confinement systems like tokamaks. In industry, MHD pumps transport conductive fluids like molten metals without mechanical components, and in biomedical fields, magnetic nanoparticles guided by magnetic fields are used for targeted drug delivery. The study of hybrid nanofluids such as  $Fe_3O_4$  and  $Al_2O_3$  in MHD systems further enhances thermal and electrical properties, making them vital for advanced energy systems, biomedical applications, and efficient cooling technologies. Patil et al. [27] revealed the Newtonian heating effect in unsteady mixed convective flow caused by a moving vertical plate. They analyzed that skin friction and convection parameters increase the temperature. Akbar and Khan [28] deliberated on the influence of magnetic fields with Newtonian heating. Refs. [29] - [30] analyzed the effects of Newtonian heating with different types of MHD flow characteristics.

The novelty of this paper lies in its comprehensive 3D analysis of hybrid nanofluids  $Fe_3O_4/Al_2O_3$  under the influence of buoyancy, Hall current, and rotation effects, which have not been thoroughly explored in prior studies. Unlike traditional nanofluid models, this research integrates the enhanced thermal properties of hybrid nanofluids, making them more relevant to industrial

applications requiring efficient heat dissipation. The paper goes beyond existing studies by introducing complex phenomena such as nonlinear thermal radiation, Joule heating, and chemical reactions, which significantly impact the fluid's thermal and dynamic behavior in real-world conditions. Furthermore, the addition of thermophoresis and Brownian motion provides a detailed understanding of nanoparticle dynamics in a stretched plate configuration. The use of similarity transformations and the shooting method for solving the nonlinear ordinary differential equations allows for accurate numerical solutions, contributing to the field of computational fluid dynamics. Moreover, this study extends the work of Essam et al. [31] by incorporating mixed convection flow and the concentration equation, providing a more robust analysis of heat and mass transfer interactions. The findings demonstrate that increased hybrid nanoparticle concentration enhances fluid flow and heat dissipation, offering new insights into optimizing heat transfer processes in various industries.

## 2 Formulation of the problem

We consider the flow of a rotating, electrically conducting fluid containing hybrid nanoparticles ( $Fe_3O_4$  and  $Al_2O_3$ ). The flow occurs over a stretched plate, and several physical effects are acting on the system. The fluid flows with a uniform velocity ( $U_w$ ) parallel to the plate, as shown by the arrows along the  $x$ -axis. This suggests that the fluid has been uniformly accelerated along the plate's surface. The system is subjected to a rotational motion characterized by a constant angular velocity ( $\omega$ ), which acts about the  $z$ -axis. This rotation can introduce Coriolis forces and influence the velocity distribution in the fluid. The fluid contains  $Fe_3O_4/Al_2O_3$  hybrid nanoparticles. These nanoparticles have unique thermal and electromagnetic properties, affecting the heat transfer and magnetic behavior of the system. Nonlinear thermal radiation is applied to the system. The radiation acts as an energy source and affects the heat flux within the fluid.  $q_r$  denotes the radiative heat flux, which can influence the temperature distribution. A uniform magnetic field of intensity  $B_0$  is applied to the plate (along the  $z$ -axis). This magnetic field will interact with the electrically conducting fluid, inducing electromagnetic forces (Lorentz force) that affect the fluid's motion. The presence of a Hall current indicates that the magnetic field generates an electric current in the fluid. This further complicates the electromagnetic interactions within the fluid and impacts the overall flow behavior. The temperature at the plate surface is denoted as  $T_w$ , while  $T_\infty$  represents the temperature of the fluid far away from the surface. This temperature gradient drives heat transfer between the plate and the fluid as shown in Figure 1. The flow equations that are used to define the model were written by Essam et al. [31].

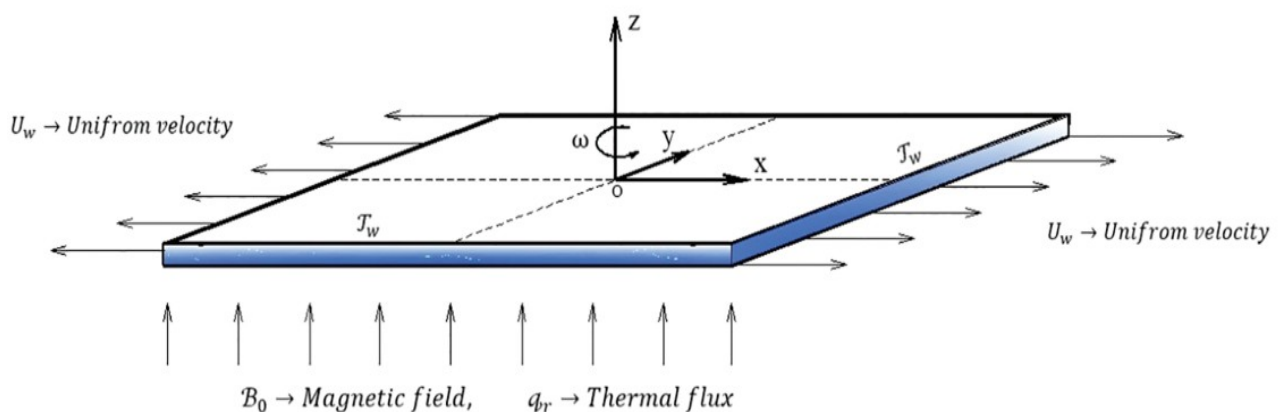


Figure 1. Analyses of geometry interpretation

$$\frac{\partial u}{\partial x} + \frac{\partial v}{\partial y} + \frac{\partial w}{\partial z} = 0, \quad (1)$$

$$\rho_{hnf} \left( u \frac{\partial u}{\partial x} + v \frac{\partial u}{\partial y} + w \frac{\partial u}{\partial z} - 2\omega v \right) = \mu_{hnf} \frac{\partial^2 u}{\partial z^2} - \frac{\sigma_{hnf} B_0^2}{(1+m^2)} (u - mv) + g [\beta_T (T - T_\infty) + \beta_c (C - C_\infty)] - \frac{\vartheta_f}{k} u, \quad (2)$$

$$\rho_{hnf} \left( u \frac{\partial v}{\partial x} + v \frac{\partial v}{\partial y} + w \frac{\partial v}{\partial z} + 2\omega u \right) = \mu_{hnf} \frac{\partial^2 v}{\partial z^2} - \frac{\sigma_{hnf} B_0^2}{(1+m^2)} (v + mu) + \frac{\vartheta_f}{k} v, \quad (3)$$

$$(\rho c_p)_{hnf} \left( u \frac{\partial T}{\partial x} + v \frac{\partial T}{\partial y} + w \frac{\partial T}{\partial z} \right) = k_{hnf} \left( \frac{\partial^2 T}{\partial z^2} \right) + \tau_{hnf} \left( D_B \frac{\partial C}{\partial z} + \frac{D_T}{T_\infty} \frac{\partial T}{\partial z} \right) \frac{\partial T}{\partial z} + \frac{\partial^2 T^4}{\partial z^2} \left( \frac{4\sigma^*}{3\alpha^*} \right) + \sigma_{hnf} B_0^2 (u^2 + v^2), \quad (4)$$

$$u \frac{\partial C}{\partial x} + v \frac{\partial C}{\partial y} + w \frac{\partial C}{\partial z} = \beta_{hnf} \left( \frac{\partial^2 C}{\partial z^2} \right) - K_C (C - C_\infty)^n. \quad (5)$$

In this particular flow, the boundary conditions that are suitable are as follows

$$\begin{aligned} w = 0, u = U_w, v = 0, T = T_w, C = C_w \quad \text{at } z = 0, \\ w \rightarrow 0, u \rightarrow 0, v \rightarrow 0, T \rightarrow T_\infty, C \rightarrow C_\infty \quad \text{at } z \rightarrow \infty. \end{aligned} \quad (6)$$

An overview of the practical properties of hybrid nanofluid is provided below. One may get more information on these qualities in [31] and the references therein.

$$\begin{aligned} \frac{\mu_{hnf}}{\mu_f} &= \left( \frac{(1-\phi_1)^{-2.5}}{(1-\phi_2)^{2.5}} \right), \\ \rho_{hnf} &= (1-\phi_2)(1-\phi_1)\rho_f - (1-\phi_2)\rho_{s1} + \phi_2\rho_{s2}, \end{aligned}$$

$$(\rho c_p)_{hnf} = (1-\phi_2)(\rho c_p)_f [(1-\phi_1) + (\rho c_p)_{s1}(1-\phi_2)] + (\rho c_p)_{s2},$$

$$k_{nf} = k_f \left( \frac{\kappa_{s1} + 2\kappa_f - 2\phi_1(\kappa_f - \kappa_{s1})}{\kappa_{s1} + 2\kappa_f + \phi_1(\kappa_f - \kappa_{s1})} \right),$$

$$k_{hnf} = k_{nf} \left( \frac{\kappa_{s2} + 2\kappa_{bf} - 2\phi_2(\kappa_{bf} - \kappa_{s2})}{\kappa_{s2} + 2\kappa_{bf} + \phi_2(\kappa_{bf} - \kappa_{s2})} \right),$$

$$\sigma_{nf} = \sigma_f \left[ \frac{\sigma_{s1} + 2\sigma_f - 2\phi_1(\sigma_f - \sigma_{s1})}{\sigma_{s1} + 2\sigma_f + \phi_1(\sigma_f - \sigma_{s1})} \right],$$

$$\sigma_{hnf} = \sigma_{nf} \left[ \frac{\sigma_{s2} + 2\sigma_{bf} - 2\phi_2(\sigma_{bf} - \sigma_{s2})}{\sigma_{s2} + 2\sigma_{bf} + \phi_2(\sigma_{bf} - \sigma_{s2})} \right].$$

Nano-solid-particles, base fluid, and hybrid nanofluid are each represented by the subscripts  $s1$ ,  $s2$ ,  $nf$ , and  $hnf$ , respectively, in this context. The percentages of solid volume that come from  $Fe_3O_4/Al_2O_3$  are represented by the symbols  $\phi_1$  and  $\phi_2$ , respectively. It is indicated in Table 1 that this is the case. The use of dimensionless numbers is a technique that is often utilized in the area of mathematical analysis as a means of simplifying problems. A similarity inversion is the method that is used in order to achieve the procedure of transforming dimensional partial differential

**Table 1.** The thermophysical characteristics of water, iron oxide, and aluminum oxide discussed in [31, 32]

Physical properties	water (H <sub>2</sub> O)	Fe <sub>3</sub> O <sub>4</sub>	Al <sub>2</sub> O <sub>3</sub>
$\rho \left( \frac{kg}{m^3} \right)$	997.100	05180.00	03970.00
$\sigma \left( \Omega^{-1} m^{-1} \right)$	$025 \times 10^{-2}$	$025 \times 10^3$	$035 \times 10^6$
$C_p \left( (kg)^{-1} J K^{-1} \right)$	4179.00	0670.00	0765.00
$k \left( W m^{-1} K^{-1} \right)$	0.61300	09.700	040.00

equations into determinate ordinary differential equations.

$$u = f'(\eta)bx, v = g(\eta)bx, w = -(f(\eta) + g(\eta))\sqrt{bv_f}, T = T_\infty\theta(\eta)\Delta T, \eta = \sqrt{\frac{b}{v_f}}z, \quad (7)$$

$$\theta(\eta) = \frac{(T-T_\infty)}{(T_w-T_\infty)}, \phi(\eta) = \frac{(C-C_\infty)}{(C_w-C_\infty)}.$$

By introducing Eq. (7) into Eqs. (2), (3), (4), and (5), it is feasible to build a set of non-linear ordinary differential equations. This is a procedure that may be carried out.

$$\left(\frac{l_4}{l_1}\right) f''' + ff'' + 2\lambda_1g - f'^2 - \left(\frac{l_5}{l_1}\right) \left(\frac{M}{(1+m^2)}\right) (f' - mg) + \lambda(\theta + N) - k_1f' = 0, \quad (8)$$

$$\left(\frac{l_4}{l_1}\right) g'' + fg' - f'g - 2\lambda_1g - \left(\frac{l_5}{l_1}\right) \left(\frac{M}{(1+m^2)}\right) (g + mf') + k_1g' = 0, \quad (9)$$

$$\theta'' + \left(\frac{Rd}{l_3}\right) [1 + (\theta_w - 1)\theta]^3\theta'' + Pr \left(\frac{l_2}{l_3}\right) (f\theta' + Nb\theta'\phi' + Nt\theta'^2) + Pr Ec M \left(\frac{l_5}{l_3}\right) (g'^2 + f'^2) + \frac{3Rd}{l_3} (\theta_w - 1) [1 + (\theta_w - 1)\theta]^2\theta'^2 = 0, \quad (10)$$

$$\frac{1}{Sc}\phi'' + (f + g)\phi' - R_c\phi = 0. \quad (11)$$

In this context, the prime represents the differentiation, and it is represented by the equation  $\phi_2$ .

$$l_1 = \frac{\rho_{hnf}}{\rho_f}, l_2 = \frac{(\rho c_p)_{hnf}}{(\rho c_p)_f}, l_3 = \frac{k_{hnf}}{k_f}, l_4 = \frac{\mu_{hnf}}{\mu_f}, \text{ and } l_5 = \frac{\sigma_{hnf}}{\sigma_f}.$$

Following this, the updated boundary conditions that correspond to the transformation (5) are as follows:

$$f(\eta) = 0, g(\eta) = 0, f'(\eta) = 1, \theta(\eta) = 1, \phi(\eta) = 1 \text{ at } z = 0, \quad (12)$$

$$f'(\eta) \rightarrow 0, g(\eta) \rightarrow 0, v \rightarrow 0, \theta(\eta) \rightarrow T_\infty, \phi(\eta) \rightarrow C_\infty \text{ at } z \rightarrow \infty.$$

In this context, prime refers to the differentiation that occurs with regard to the primary thermo-

dynamic physical characteristics that exhibit the flow dynamics.

$$\begin{aligned} \lambda_1 &= \frac{\omega}{b}, M = \frac{\sigma_f B_0^2 x}{\rho_f b}, \text{Pr} = \frac{\nu_f}{k_f} = \frac{(\nu \rho C_p)_f}{k_f}, \theta_w = \frac{T_w}{T_\infty}, Ec = \frac{u^2 \rho_f}{(\rho C_p)_f (T - T_\infty)}, \\ Rd &= \frac{16 \sigma^* T_\infty^3}{3 k_f \alpha^*}, Rc = \frac{K_c k_T (C - C_\infty)^{n-1}}{b}, Nb = \frac{\tau D_B (C_w - C_\infty)}{\nu}, Nt = \frac{\tau D_T (T_w - T_\infty)}{\nu T_\infty}, \\ \lambda &= \frac{g [\beta_T (T - T_\infty) (1 - Ct)^2]}{a^2 x}, N = \frac{\beta_c (C - C_\infty)}{\beta_T (T - T_\infty)}, k_1 = \frac{\nu}{ka} (1 - Ct), Sc = \frac{\nu_f}{\beta_f}. \end{aligned} \quad (13)$$

### 3 Physical quantities of interests

In this context, the skin friction along the x and y axes is represented by the symbols  $Cf_x$  and  $Cf_y$  the local Nusselt number is represented by the symbol  $Nu_x$ , and the Sherwood number is represented by the symbol  $Sh_x$ .

$$\begin{aligned} Cf_x &= \frac{\mu_{mf}}{\rho_f (bx)^2} \left( \frac{\partial u}{\partial z} \right)_{z=0}, Cf_y = \frac{\mu_{mf}}{\rho_f (bx)^2} \left( \frac{\partial v}{\partial z} \right)_{z=0}, \\ Nu_x &= - \frac{x k_{mf}}{k_f (T - T_\infty)} \left( \frac{\partial T}{\partial z} \right)_{z=0}, \\ Sh_x &= \frac{x k_{mf}}{k_f (C - C_\infty)} \left( \frac{\partial C}{\partial z} \right)_{z=0}. \end{aligned} \quad (14)$$

The following provides an illustration of the factor of skin friction, the Nusselt digit, and the number determined by Sherwood in their relevant non-dimensional geometries and in the context of the similitude variable. These representations are supplied in the following paragraphs.

$$\begin{aligned} \text{Re}_x^{1/2} Cf_x &= \frac{\mu_{mf}}{n_f} f''(0), \text{ and } \text{Re}_x^{1/2} Cf_y = \frac{\mu_{mf}}{n_f} g''(0), \\ \text{Re}_x^{-1/2} Nu_x &= - \left( \frac{k_{mf}}{k_f} + Rd \theta_w \right) \theta'(0), \\ \text{Re}_x^{-1/2} Sh_x &= - \frac{k_{mf}}{k_f} \phi(0). \end{aligned} \quad (15)$$

### 4 Method of solution

In all cases, the set of nonlinear coupled ordinary differential equations (ODEs) (8)-(12) has been numerically solved using the fourth-order Runge-Kutta method combined with a shooting strategy. The program utilized for this purpose is MATLAB, with a step size of  $\nabla \eta = 0.01$  and an error limit of  $10^{-6}$ . By incorporating additional variables, the nonlinear ODEs are transformed into a system of linear first-order ODEs, which is one of the advantages of this method. In the second stage of the procedure, the boundary value problem is converted into an initial value problem by assigning guessed values to the unknown starting values according to the specific requirements of the problem at hand. The shooting method then adjusts these estimated values to align with the defined boundary conditions. After the necessary number of iterations to refine the guessed values, forward integration is performed to provide numerical solutions for the desired points and intervals. However, certain restrictions apply: some partial differential equations (PDEs) that describe the governing equations do not admit similarity transformations and cannot be converted into ODEs. Only specific types of flow problems are suitable for similarity transformations, leading to comparable solutions. Additionally, a particular problem may have multiple solutions; in such cases, it is essential to select the most reliable solution and discuss the rationale behind this choice. To assess the accuracy of the present code and validity check, the numerical values of  $f''(0)$ ,  $g'(0)$  and  $Nu_e \text{Re}_x^{-1/2}$  are presented in Table 2 and Table 3. From the Table 2, the comparison of velocity

values for the rotation parameter at 0.50, 1.00, and 2.00 reveals a strong agreement between the results of the current study and those reported in previous studies by [31] and Abdel-Wahed [33]. Specifically, at  $\lambda = 0.50$  the current study's results (-1.14576) are closely aligned with both Abdel-Wahed (-1.13874) and Essam et al. (-1.13830), indicating a consistent trend in the velocity profiles. Similarly, at  $\lambda = 1.00$ , the values are nearly identical, with the current study showing -1.32452 compared to -1.32503 and -1.32505 from the previous studies. Finally, at  $\lambda = 2.00$ , the current study's result of -1.64574 remains in close proximity to the values of -1.62232 and -1.65233 from the earlier works. This good agreement across the rotation parameter values suggests that the methodologies and assumptions used in our study are valid and that the results are reliable. The consistency also reinforces the credibility of the underlying physics governing the flow behavior under the specified conditions, thereby validating the model employed in this analysis. Overall, these findings not only confirm the accuracy of our results but also enhance the understanding of the dynamics involved in the flow under the influence of rotation.

**Table 3** presents a comparison of results for various values of the rotation parameter  $Rd$  and  $\theta_w$  under the conditions where  $\lambda = 0$  and  $Nb = Nt = Sc = Rc = 0$ . The data shows a close agreement between the results of the current study and those of previous studies by Essam et al. [31] and Abdel-Wahed [33].

For  $Rd = 0$  and  $\theta_w = 1.00$ , the current study reports a value of 1.867, which is very similar to the values reported by Abdel-Wahed (1.8572) and Essam et al. (1.8576). This proximity suggests that our results are consistent with established findings under these specific conditions. At  $Rd = 1.00$  and  $\theta_w = 1.00$ , the current study's result (2.234) aligns closely with those of Abdel-Wahed (2.2367) and Essam et al. (2.2364), indicating strong validation of the model and numerical methods used in this analysis. Similarly, for  $\theta_w = 1.100$  and  $\theta_w = 1.500$ , the results from the contemporary study (2.311 and 2.600, respectively) remain consistent with the values from the previous studies, with small deviations that fall within acceptable ranges.

These findings highlight the reliability of the current study's results and reinforce the accuracy of the methodologies employed. The close alignment with prior research not only validates the numerical techniques used but also enhances the understanding of the underlying physical phenomena being investigated. Overall, this agreement underscores the robustness of the results obtained in this study.

The results of the numerical simulations for the rate coefficients, which include the shear rate and the heat transfer rate, have been generated and are shown in **Table 4** for the modification of various contributing components. In conclusion, the results of the simulations have been produced. The higher values of the nanoparticle concentration, magnetic parameter, and thermal buoyancy all contribute significantly to the rise in the rate of shear stress, as shown by the findings of the research. Additionally, the concentrations of nanoparticles of ( $Fe_3O_4$  and  $Al_2O_3$ ) both increase the magnitude of the rate of heat transfer; nevertheless, the other contributing elements have a retarding impact on the profile of the rate of heat transfer. This is because the nanoparticles of these two materials are composed of nanoparticles.

## 5 Results and discussion

When a boundary layer is being simulated on a stretched plate, it is being done so under the effect of a spinning hybrid nanofluid that is composed of ( $Fe_3O_4/Al_2O_3$ ) nanoparticles and water as the base fluid. The nanofluid that has been created is a combination of two different types of nanoparticles that have been blended. For the purpose of this study, the effect of a number of different elements, including the magnetic field, the Hall current, the rotation parameter, the Brownian motion parameter, the thermophoresis parameter, Joule heating, and nonlinear thermal radiation, was investigated across the boundary layer. The effective completion of this assignment



was made possible by making use of Figure 2 to Figure 23 throughout the method. For the purpose of determining the magnitude of the transversal velocity, the y-axis is employed, whereas the x-axis is utilized for the purpose of determining the magnitude of the longitudinal velocity. In addition, Table IV provides an illustration of the influence that each of the components that were used has on the movement of heat and the friction that takes place on the surface that surrounds the environment. A subsequent part will be devoted to the presentation of an analysis and interpretation of the data that were obtained.

Diagrammatic representation of the velocity field for a variety of magnetic values ( $M$ ) is shown in Figure 2, Figure 3 and Figure 4 consequently. Figure 2 depicts the pattern of a decrease in the velocity of the liquid as the quantity of  $M$  enhances. An increase in the magnitude of the magnetic factor results in the production of a resistive force that is often referred to as the Lorentz force. This Lorentz force serves to impede the velocity of the liquid, resulting in a decrease in the velocity of the liquid. As a result, a physical phenomenon taking place in which the velocity distribution decreases occurs whenever the quantity of  $M$  increases. The reversal behavior has been observed in the case of longitudinal and temperature fields.

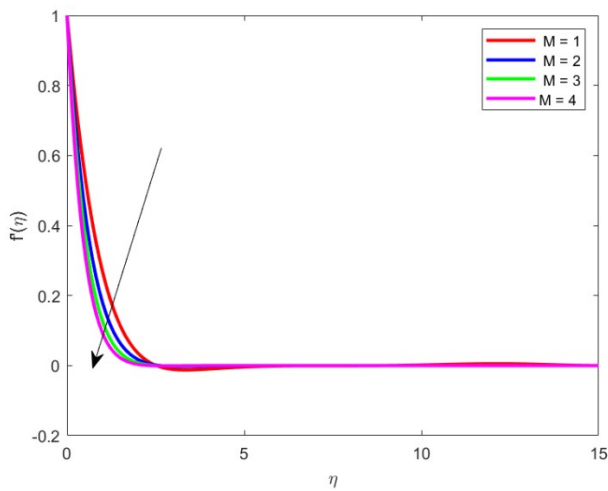


Figure 2. The consequence of  $M$  on  $f'(\eta)$

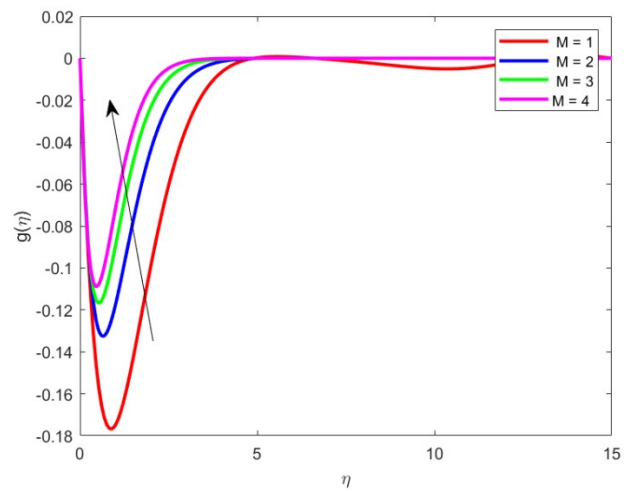


Figure 3. The consequence of  $M$  on  $g(\eta)$

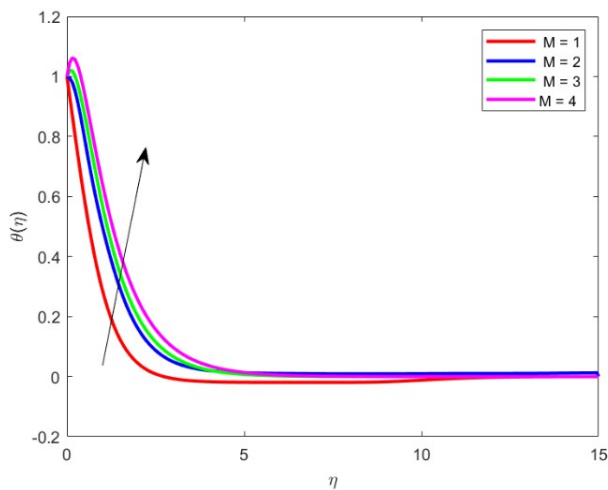


Figure 4. The consequence of  $M$  on  $\theta(\eta)$

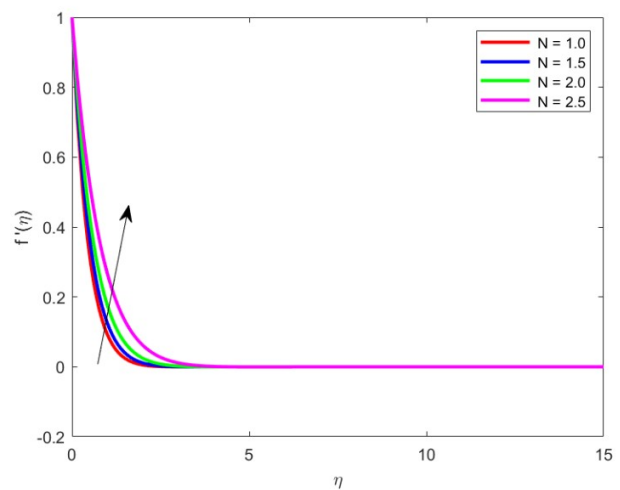
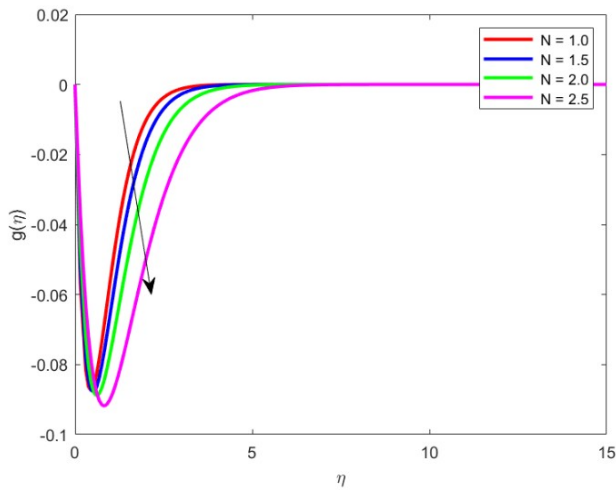
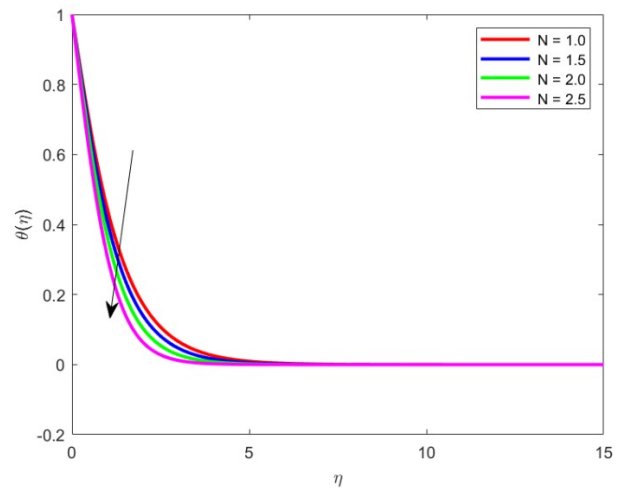


Figure 5. The consequence of  $N$  on  $f'(\eta)$



**Figure 6.** The consequence of  $N$  on  $g(\eta)$



**Figure 7.** The consequence of  $N$  on  $\theta(\eta)$

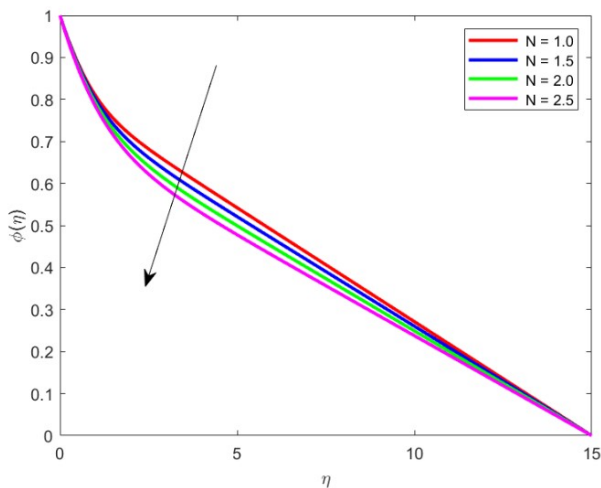


**Figure 8.** The consequence of  $N$  on  $\phi(\eta)$

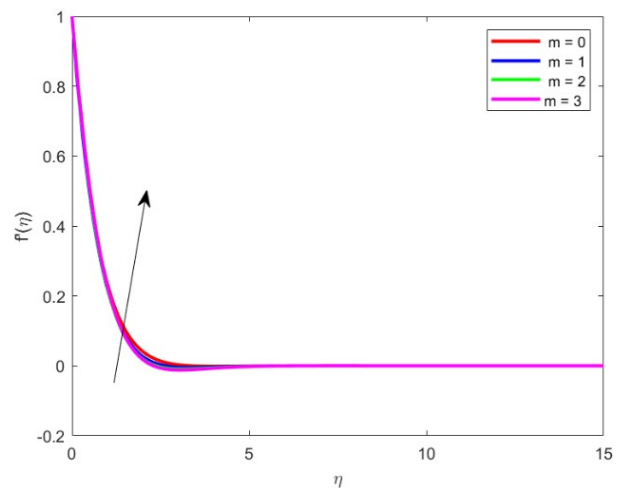


**Figure 9.** The consequence of  $m$  on  $f'(\eta)$

Figure 5, Figure 6, Figure 7 and Figure 8 depict the impact of buoyancy on velocity, temperature, and concentration profiles. The paragraph describes the physical implications of buoyancy on fluid velocity, temperature distribution, and concentration gradients. When buoyancy increases, it enhances the primary velocity of the fluid. However, this intensified primary velocity causes a decrease in the secondary velocity component. As a result, the temperature and concentration profiles across the fluid domain are also reduced. This suggests that buoyancy plays a significant role in altering the flow characteristics and thermal behavior of the fluid, ultimately influencing its overall transport properties.

The presence of a Hall current, generated by a strong magnetic field, leads to Joule heating, which subsequently increases both the thickness of the thermal boundary layer and the temperature within it. The influence of the Hall current parameter  $m$  on longitudinal and transverse velocity profiles is illustrated in Figure 9 and Figure 10. Specifically, the results in Figure 9 indicate that an increase in the Hall current parameter correlates with a rise in the longitudinal velocity within the fluid's temperature profile. Additionally, Figure 10 depicts the effects of the Hall parameter  $m$  on transverse momentum, revealing an inverse relationship between the Hall parameter and

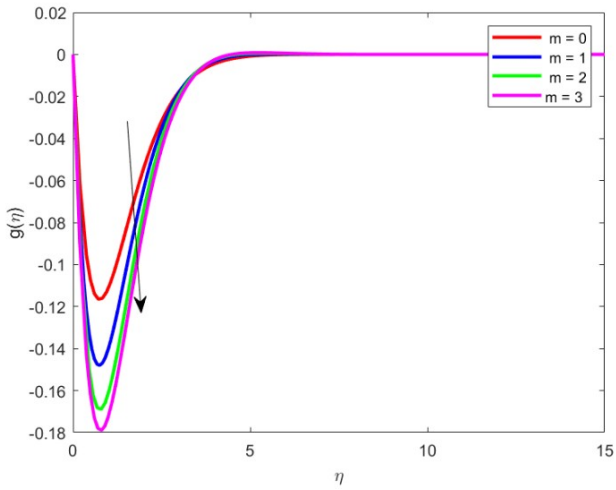


Figure 10. The consequence of  $m$  on  $g(\eta)$

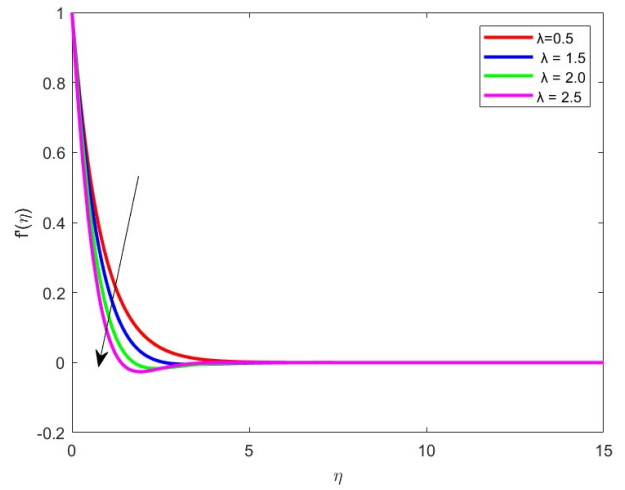


Figure 11. The consequence of  $\lambda$  on  $f'(\eta)$

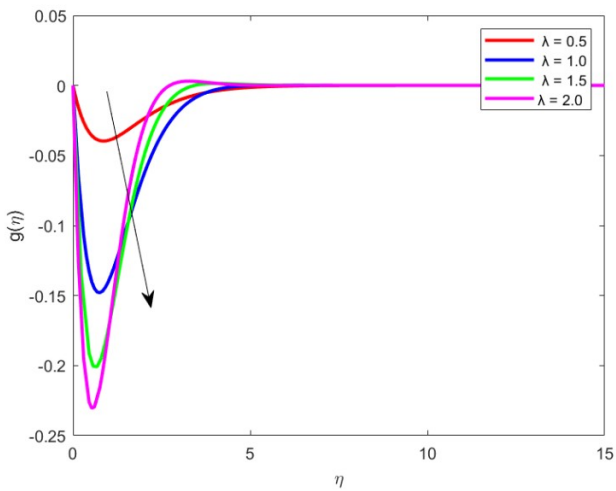


Figure 12. The consequence of  $\lambda$  on  $g(\eta)$

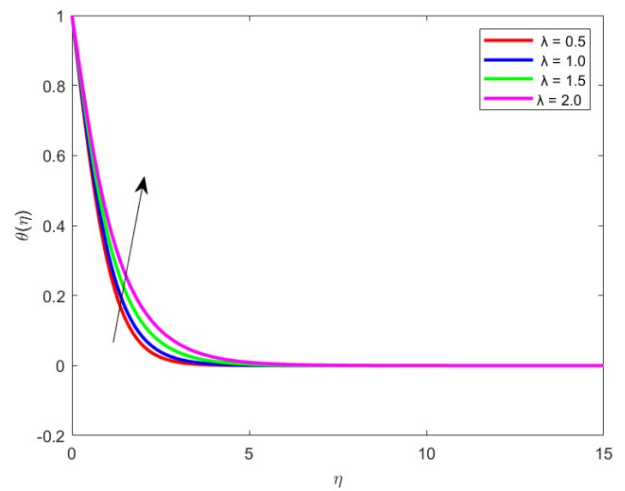


Figure 13. The consequence of  $\lambda$  on  $\theta(\eta)$

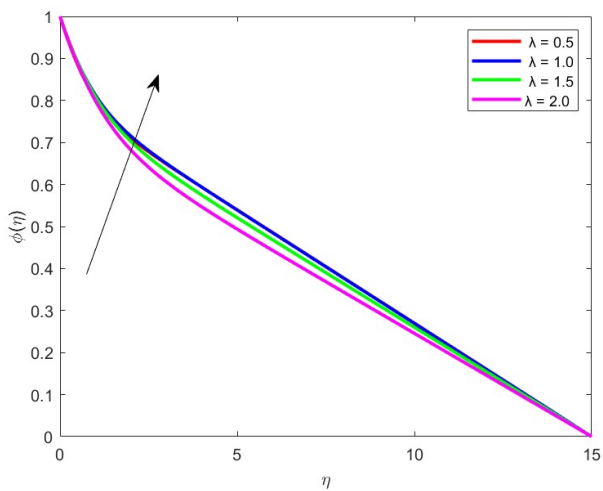


Figure 14. The consequence of  $\lambda$  on  $\phi(\eta)$

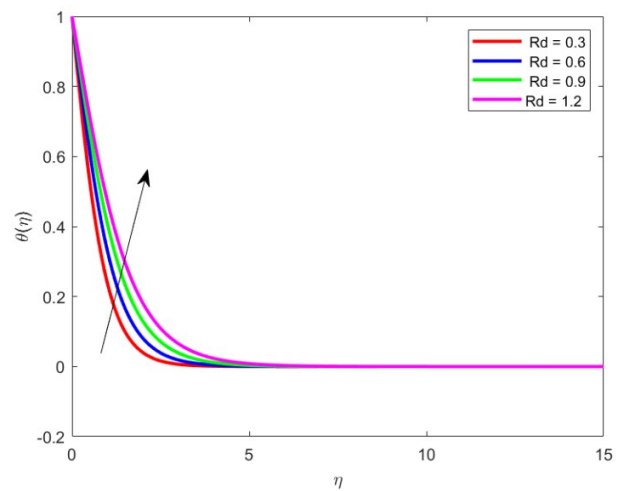
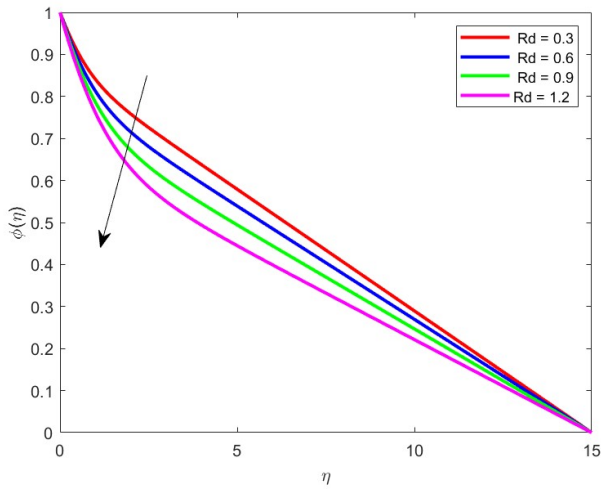
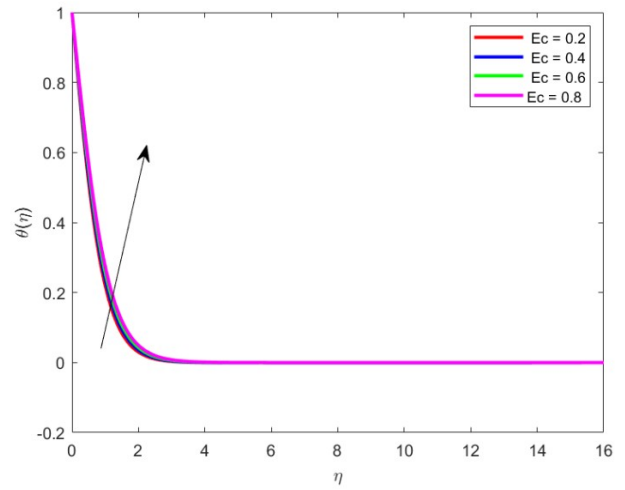


Figure 15. The consequence of  $Rd$  on  $\theta(\eta)$



**Figure 16.** The consequence of  $Rd$  on  $\phi(\eta)$



**Figure 17.** The consequence of  $Ec$  on  $\theta(\eta)$

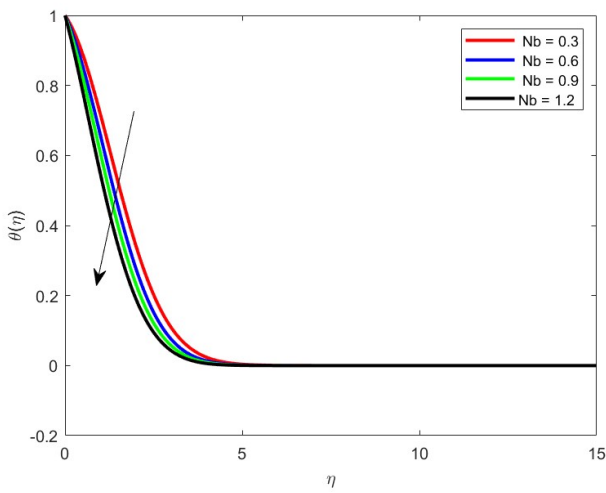


**Figure 18.** The consequence of  $Nb$  on  $\theta(\eta)$

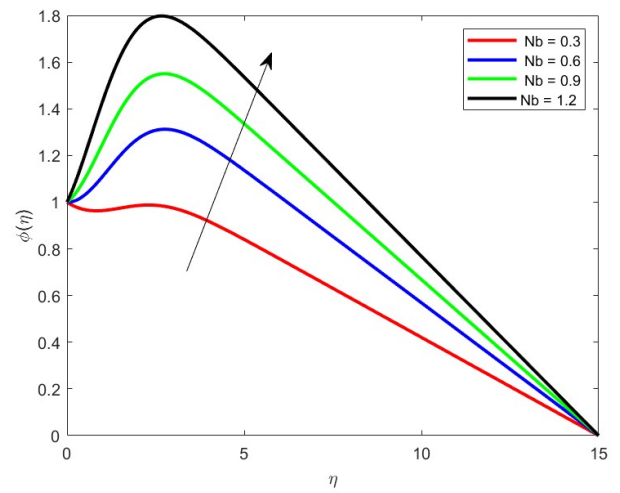


**Figure 19.** The consequence of  $Nb$  on  $\phi(\eta)$

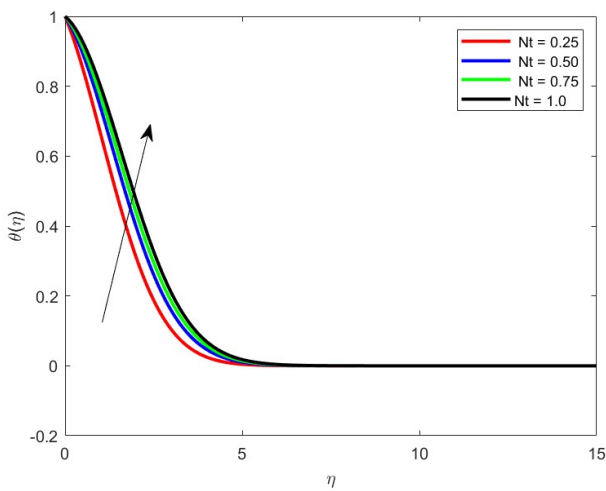


**Figure 20.** The consequence of  $Nt$  on  $\theta(\eta)$

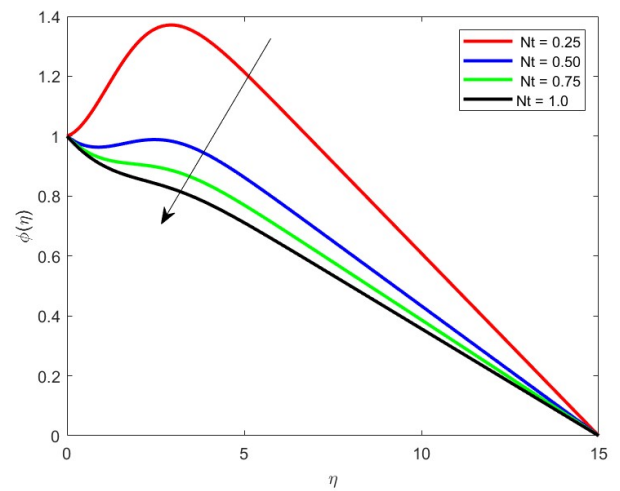


**Figure 21.** The consequence of  $Nt$  on  $\phi(\eta)$

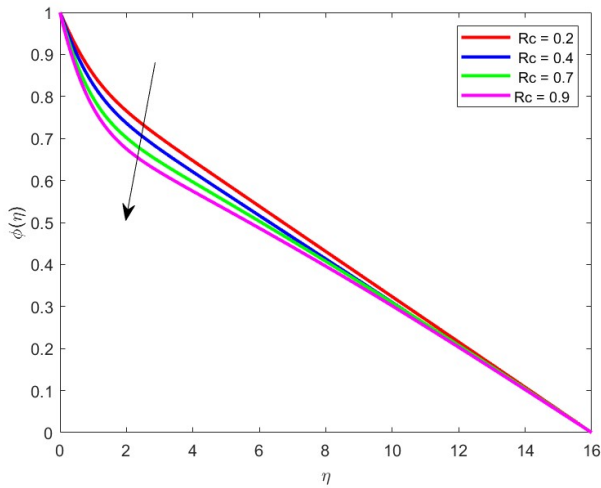


Figure 22. The consequence of  $Rc$  on  $\phi(\eta)$

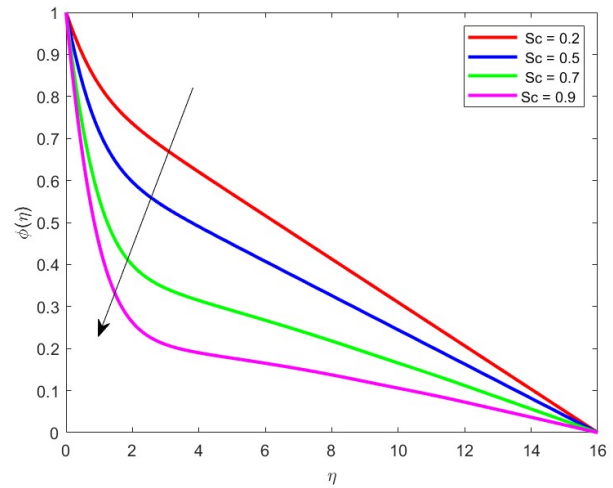


Figure 23. The consequence of  $Sc$  on  $\phi(\eta)$

transverse velocity. This inverse dynamic has been confirmed through careful observation and analysis.

The influence of the rotation factor on longitudinal velocity is illustrated in Figure 11. The rotation parameter, commonly denoted as  $\lambda$ , indicates that a high rotation rate is associated with increased longitudinal acceleration, which ultimately exceeds the stretching rate. An increase in the rotation parameter leads to enhanced centrifugal force, resulting in pressure being exerted on the fluid. This pressure causes the liquid to experience greater radial movement than under other conditions. Figure 12 visually represents the impact of the rotation parameter on forward velocity in the longitudinal direction. Additionally, data analysis indicates that higher transverse acceleration is linked to improved values, as depicted in Figure 13 and Figure 14.

Figure 15 and Figure 16 illustrate the impact of the radiation factor on temperature and concentration distribution. These graphs show that both the acceleration and temperature of the liquid increase as the radiation factor is amplified. Physically, this radiation enhances surface heat flow, leading to a higher expected temperature in the boundary layer. In contrast, the concentration consistently exhibits a decreasing trend as the radiation factor increases.

The role of the Eckert number ( $Ec$ ) is crucial in these effects. Figure 17 visually represents how the temperature field responds to changes in the Eckert number. An increase in the Eckert number results in a rise in the temperature field, highlighting a direct relationship. This indicates that regardless of the magnitude of the increase in  $Ec$ , the temperature will also rise accordingly.

Table 2. Comparison of  $f''(0), g'(0)$  with a previous studied when  $\lambda = 0, Nb = Nt = Rc = 0$

$\lambda$	Abdel-wahed [33]		Essam et al [31]		Present Result	
	$f''(0)$	$g'(0)$	$f''(0)$	$g'(0)$	$f''(0)$	$g'(0)$
0.50	-1.13874	-0.51273	-1.13830	-0.51275	-1.14576	-0.509788
1.0	-1.32503	-0.83714	-1.32505	-0.83717	-1.32452	-0.834575
2.0	-1.62232	-1.28728	-1.65233	-1.28720	-1.64574	-1.277851

The influence of the Brownian motion factor  $Nb$  on velocity and temperature profiles is shown in

**Table 3.** Comparison of  $Re_x^{-1/2} Nu_x$  with a previous studied when  $\lambda = 0, Nb = Nt = Sc = RC = 0$

$Rd$	$\theta_w$	Abdel-wahed [33]	Essam et al [31]	Contemporary Study
0.0	1.0	1.8572	1.8576	1.867
1.00	1.0	2.2367	2.2364	2.234
1.00	1.100	2.3044	2.3043	2.311
1.00	1.500	2.6086	2.6083	2.600

**Table 4.** The rate coefficients exhibit a significant behaviour with respect to the parameters

$\phi_1$	$\phi_2$	$M$	$m$	$Ec$	$Rd$	$Nb$	$Nt$	$Cf_x$	$Cf_y$	$Nu_x$
0	0.01	0.5	1.0	0.001	0.5	0.5	0.5	-0.98686	1.23141	1.27615
0.10								-0.99191	1.74131	1.43121
0.20								-1.01928	1.97562	1.76151
	0.10							-1.25242	1.62524	1.87252
	0.20							-0.98712	1.24231	1.62332
		0.10						-0.12635	1.65242	1.73635
		0.20						-0.98173	1.78267	1.52363
			0.20					-0.82753	1.28363	1.65343
			0.40					-0.99835	1.56727	1.43534
				0.20				-0.27454	1.53737	1.75634
				0.40				-0.75637	1.67383	1.25353
					0.20			-0.86454	1.53436	1.09637
					0.40			-0.64364	1.45353	0.98367
						0.5		-0.98752	1.21421	1.01245
						1.0		-0.54752	1.10214	1.22457
							0.30	-0.75421	1.22545	1.54878
							0.30	-0.22101	1.00124	1.65475

**Figure 18** and **Figure 19**. As  $Nb$  increases from 0.3 to 1.2, the velocity in the boundary layer decreases, as seen in **Figure 18**. Meanwhile, **Figure 19** demonstrates that dimensionless temperature rises with increasing  $Nb$  due to more frequent collisions among nanofluid particles, which generate thermal energy and elevate the nanofluid temperature. The analysis of the thermophoresis parameter  $Nt$  reveals its significant impact. As illustrated in **Figure 20** and **Figure 21**, increasing  $Nt$  raises both the boundary layer temperature and the concentration of nanoparticles. Increasing  $Nt$  from 0.25 to 1.0 also enhances the velocity and temperature of nanoparticles at the surface. The thermophoresis parameter can have positive or negative values; a negative value indicates a hot surface, while a positive value signifies a cold surface.

The primary focus in this context is the conversion of mechanical energy into thermal energy. The observed phenomenon can be attributed to thermal energy dissipation. This is illustrated in **Figure 22**, which shows the impact of the chemical reaction parameter  $Rc$  on concentration. There is a clear correlation where an increase in  $Rc$  leads to a reduction in the concentration of perimeter coating.

**Figure 23** visually represents the effect of the Schmidt factor on the concentration profile. It has been established that mass diffusivity and momentum diffusivity are interconnected. As the Schmidt factor decreases, the concentration profile also diminishes, resulting in a thinner concentration boundary layer in the mixed nanoparticles hybrid nanofluid.

## 6 Conclusion

- The velocity of the liquid decreases as the magnetic value ( $M$ ) increases, due to the Lorentz force acting as a resistive force that impedes flow. This results in a diminishing velocity distribution and a reversal behavior is also observed in the longitudinal and temperature fields.
- Buoyancy significantly impacts fluid dynamics. As it increases, the primary velocity rises while the secondary velocity decreases, leading to reduced temperature and concentration profiles. This alteration affects the fluid's overall transport properties.
- The Hall current generated by a strong magnetic field causes Joule heating, increasing the thickness of the thermal boundary layer and the temperature within it. An increase in the Hall current parameter ( $m$ ) enhances the longitudinal velocity, while its relationship with transverse velocity is inversely correlated, as observed through careful study.
- The rotation factor, significantly influences longitudinal velocity, with higher rotation rates leading to greater longitudinal acceleration, often exceeding stretching rates. Increased rotation generates centrifugal forces that apply pressure to the fluid, causing particles to move radially faster than under other conditions. A higher transverse acceleration is also associated with improved values.
- Additionally, increased radiation enhances both liquid temperature and acceleration, as radiation boosts surface heat flow, raising temperatures in the boundary layer. In contrast, concentration tends to decrease.
- The Eckert number ( $Ec$ ) plays a crucial role in these effects, with rising values correlating with increased temperature fields.
- As Brownian Motion Factor ( $Nb$ ) increases from 0.3 to 1.2, the boundary layer velocity decreases, while the dimensionless temperature rises due to more frequent collisions among nanofluid particles generating thermal energy.
- Increasing Thermophoresis parameter ( $Nt$ ) leads to higher boundary layer temperatures and nanoparticle concentrations, as well as enhanced velocity and temperature at the surface. The sign of  $Nt$  indicates surface temperature conditions, with negative values suggesting hot surfaces.
- An increase in Chemical Reaction Parameter  $Rc$  correlates with a reduction in concentration, indicating that higher reaction rates lead to decreased concentration levels in the fluid.
- A lower Schmidt factor reduces the concentration profile, resulting in a thinner concentration boundary layer in the mixed nanoparticles hybrid nanofluid, reflecting a connection between mass and momentum diffusivity.

### Declarations

#### Use of AI tools

The authors declare that they have not used Artificial Intelligence (AI) tools in the creation of this article.

#### Data availability statement

No Data associated with the manuscript.

#### Ethical approval (optional)

The authors state that this research complies with ethical standards. This research does not involve either human participants or animals.

### Consent for publication

Not applicable

### Conflicts of interest

The authors declare that they have no conflict of interest.

### Funding

No funding was received for this research.

### Author's contributions

K.N.V.Ch.B.: Conceptualization, Methodology, Data curation, Formal analysis, Writing of the original draft, Reviewing and editing. S.M.I.: Conceptualization, Methodology, Data curation, Formal analysis, Writing of the original draft, Reviewing and editing. R.K.: Conceptualization, Methodology, Data curation, Formal analysis, Writing of the original draft, Reviewing and editing. All authors have read and approved the final manuscript.

### Acknowledgements

Not applicable

### References

- [1] Khan, U., Ullah, B., Khan, W., Adnan, Khan, I. and Fayz-Al-Asad, M. Applied mathematical modelling and heat transport investigation in hybrid nanofluids under the impact of thermal radiation: numerical analysis. *Mathematical Problems in Engineering*, 2021(1), 180513, (2021). [[CrossRef](#)]
- [2] Adnan, Khan, U., Ahmed, N., Mohyud-Din, S.T., Khan, I. and Fayz-Al-Asad, M. The numerical investigation of the heat transport in the nanofluids under the impacts of magnetic field: applications in industrial zone. *Mathematical Problems in Engineering*, 2021(1), 3138301, (2021). [[CrossRef](#)]
- [3] Ullah, H., Khan, I., Fiza, M., Hamadneh, N.N., Fayz-Al-Asad, M., Islam, S. et al. MHD boundary layer flow over a stretching sheet: A new stochastic method. *Mathematical Problems in Engineering*, 2021(1), 9924593, (2021). [[CrossRef](#)]
- [4] Kumar, R., Sood, S., Shehzad, S.A. and Sheikholeslami, M. Radiative heat transfer study for flow of non-Newtonian nanofluid past a Riga plate with variable thickness. *Journal of Molecular Liquids*, 248, 143-152, (2017). [[CrossRef](#)]
- [5] Fayz-Al-Asad, M., Yavuz, M., Alam, M.N., Sarker, M.M.A. and Bazighifan, O. Influence of fin length on magneto-combined convection heat transfer performance in a lid-driven wavy cavity. *Fractal and Fractional*, 5(3), 107, (2021). [[CrossRef](#)]
- [6] Hossain, M.S., Fayz-Al-Asad, M., Mallik, M.S.I., Yavuz, M., Alim, M.A. and Khairul Basher, K.M. Numerical study of the effect of a heated cylinder on natural convection in a square cavity in the presence of a magnetic field. *Mathematical and Computational Applications*, 27(4), 58, (2022). [[CrossRef](#)]
- [7] Kodi, R., Vaddemani, R.R., Kommaddi, H., Noeiaghdam, S. and Fernandez-Gamiz, U. Thermodynamic and buoyancy force effects of Cu and TiO<sub>2</sub> nanoparticles in engine oil flow over an inclined permeable surface. *Journal of King Saud University-Science*, 36(10), 103434, (2024). [[CrossRef](#)]



- 
- [8] Zhang, L., Vaddemani, R.R., Ganjikunta, A., Bingi, S. and Kodi, R. 3D-MHD mixed convection in a darcy-forchheimer maxwell fluid: Thermo diffusion, diffusion-thermo effects, and activation energy influence. *Case Studies in Thermal Engineering*, 61, 104916, (2024). [[CrossRef](#)]
- [9] Choi, S.U.S and Eastman, J.A. Enhancing thermal conductivity of fluids with nanoparticles. In Proceedings, *International Mechanical Engineering Congress & Exposition (IMECE)*, pp. 99-105, San Francisco, ABD, (199, November).
- [10] Ashorynejad, H.R., Sheikholeslami, M., Pop, I. and Ganji, D.D. Nanofluid flow and heat transfer due to a stretching cylinder in the presence of magnetic field. *Heat and Mass Transfer*, 49, 427-436, (2013). [[CrossRef](#)]
- [11] Omar, N.S., Bachok, N. and Arifin, N.M. Stagnation point flow over a stretching or shrinking cylinder in a copper-water nanofluid. *Indian Journal of Science and Technology*, 8(31), 1-7, (2015). [[CrossRef](#)]
- [12] Mabood, F., Khan, W.A. and Ismail, A.M. MHD boundary layer flow and heat transfer of nanofluids over a nonlinear stretching sheet: a numerical study. *Journal of Magnetism and Magnetic Materials*, 374, 569-576, (2015). [[CrossRef](#)]
- [13] Mabood, F. and Khan, W.A. Analytical study for unsteady nanofluid MHD Flow impinging on heated stretching sheet. *Journal of Molecular Liquid*, 219, 216-223, (2016). [[CrossRef](#)]
- [14] Khan, M.I., Khan, S.A., Hayat, T., Khan, M.I. and Alsaedi, A. Nanomaterial based flow of Prandtl-Eyring (non-Newtonian) fluid using Brownian and thermophoretic diffusion with entropy generation. *Computer Methods and Programs in Biomedicine*, 180, 105017, (2019). [[CrossRef](#)]
- [15] Khan, M.I., Hayat, T., Khan, M.I., Waqas, M. and Alsaedi, A. Numerical simulation of hydro-magnetic mixed convective radiative slip flow with variable fluid properties: a mathematical model for entropy generation. *Journal of Physics and Chemistry of Solids*, 125, 153-164, (2019). [[CrossRef](#)]
- [16] Ahmad, A., Asghar, S. and Afzal, S. Flow of nanofluid past a Riga plate. *Journal of Magnetism and Magnetic Materials*, 402, 44-48, (2016). [[CrossRef](#)]
- [17] Shah, N.A., Tosin, O., Shah, R., Salah, B. and Chung, J.D. Brownian motion and thermophoretic diffusion effects on the dynamics of MHD upper convected Maxwell nanofluid flow past a vertical surface. *Physica Scripta*, 96(12), 125722, (2021). [[CrossRef](#)]
- [18] Shah, N.A., Popoola, A.O., Oreyeni, T., Omokhuale, E. and Altine, M.M. A modelling of bioconvective flow existing with tiny particles and quartic autocatalysis reaction across stratified upper horizontal surface of a paraboloid of revolution. *Mathematical Modelling and Numerical Simulation with Applications*, 3(1), 74-100, (2023). [[CrossRef](#)]
- [19] Oreyeni, T., Oladimeji Akindede, A., Martins Obalalu, A., Olakunle Salawu, S. and Ramesh, K. Thermal performance of radiative magnetohydrodynamic Oldroyd-B hybrid nanofluid with Cattaneo–Christov heat flux model: Solar-powered ship application. *Numerical Heat Transfer, Part A: Applications*, 85(12), 1954-1972, (2023). [[CrossRef](#)]
- [20] Fayz-Al-Asad, M., Oreyeni, T., Yavuz, M. and Olanrewaju, P.O. Analytic simulation of MHD boundary layer flow of a chemically reacting upper-convected Maxwell fluid past a vertical surface subjected to double stratifications with variable properties. *The European Physical Journal Plus*, 137, 813, (2022). [[CrossRef](#)]
- [21] Yadav, D., Awasthi, M.K., Ragoju, R., Bhattacharyya, K., Kodi, R. and Wang, J. The impact of

rotation on the onset of cellular convective movement in a Casson fluid saturated permeable layer with temperature dependent thermal conductivity and viscosity deviations. *Chinese Journal of Physics*, 91, 262-277, (2024). [[CrossRef](#)]

- [22] Yedhiri, S.R., Palaparthi, K.K., Kodi, R. and Asmat, F. Unsteady MHD rotating mixed convective flow through an infinite vertical plate subject to Joule heating, thermal radiation, Hall current, radiation absorption. *Journal of Thermal Analysis and Calorimetry*, 149, 8813–8826, (2024). [[CrossRef](#)]
- [23] Kommaddi, H.B., Kodi, R., Ganteda, C. and Lorenzini, G. Heat and mass transfer on unsteady MHD chemically reacting rotating flow of Jeffrey fluid past an inclined plates under the impact of hall current, diffusion thermo and radiation absorption. *Journal of Advanced Research in Fluid Mechanics and Thermal Sciences*, 111(2), 225-241, (2023). [[CrossRef](#)]
- [24] Kodi, R., Ravuri, M.R., Veeranna, V., Khan, M.I., Abdullaev, S. and Tamam, N. Hall current and thermal radiation effects of 3D rotating hybrid nanofluid reactive flow via stretched plate with internal heat absorption. *Results in Physics*, 53, 106915, (2023). [[CrossRef](#)]
- [25] Raju, K.V., Mohanaramana, R., Reddy, S.S. and Raghunath, K. Chemical radiation and sores effects on unsteady MHD convective flow of Jeffrey nanofluid past an inclined semi-infinite vertical permeable moving plate. *Communications in Mathematics and Applications*, 14(1), 237-255, (2023). [[CrossRef](#)]
- [26] Dandu, S., Chitrapu, V.R.M. and Kodi, R. An investigation into the impact of thermal radiation and chemical reactions on the flow through porous media of a Casson hybrid nanofluid including unstable mixed convection with a stretched sheet in the presence of thermophoresis and Brownian motion. *Open Physics*, 22(1), 20240043, (2024). [[CrossRef](#)]
- [27] Patil, P.M., Anilkumar, D. and Roy, S. Unsteady thermal radiation mixed convection flow from a moving vertical plate in a parallel free stream: effect of Newtonian heating. *International Journal of Heat and Mass Transfer*, 62, 534-540, (2013). [[CrossRef](#)]
- [28] Akbar, N.S. and Khan, Z.H. Influence of magnetic field for metachronal beating of cilia for nanofluid with Newtonian heating. *Journal of Magnetism and Magnetic Materials*, 381, 235-242, (2015). [[CrossRef](#)]
- [29] Das, M., Mahato, R. and Nandkeolyar, R. Newtonian heating effect on unsteady hydromagnetic Casson fluid flow past a flat plate with heat and mass transfer. *Alexandria Engineering Journal*, 54(4), 871-879, (2015). [[CrossRef](#)]
- [30] Pal, D., Roy, N. and Vajravelu, K. Effects of thermal radiation and Ohmic dissipation on MHD Casson nanofluid flow over a vertical non-linear stretching surface using scaling group transformation. *International Journal of Mechanical Sciences*, 114, 257-267, (2016). [[CrossRef](#)]
- [31] Elsaid, E.M. and AlShurafat, K.S. Impact of hall current and joule heating on a rotating hybrid nanofluid over a stretched plate with nonlinear thermal radiation. *Journal of Nanofluids*, 12(2), 548-556, (2023). [[CrossRef](#)]
- [32] Elsaid, E.M. and Abdel-wahed, M.S. MHD mixed convection Ferro Fe<sub>3</sub>O<sub>4</sub>/Cu-hybrid-nanofluid runs in a vertical channel. *Chinese Journal of Physics*, 76, 269-282, (2022). [[CrossRef](#)]
- [33] Abdel-Wahed, M.S. Rotating ferro-nanofluid over stretching plate under the effect of hall current and joule heating. *Journal of Magnetism and Magnetic Materials*, 429, 287-293, (2017). [[CrossRef](#)]

Mathematical Modelling and Numerical Simulation with Applications (MMNSA)  
(<https://dergipark.org.tr/en/pub/mmnsa>)



**Copyright:** © 2024 by the authors. This work is licensed under a Creative Commons Attribution 4.0 (CC BY) International License. The authors retain ownership of the copyright for their article, but they allow anyone to download, reuse, reprint, modify, distribute, and/or copy articles in MMNSA, so long as the original authors and source are credited. To see the complete license contents, please visit (<http://creativecommons.org/licenses/by/4.0/>).

**How to cite this article:** Bhargava, K.N.V.Ch., Ibrahim, S.M. and Kodi, R. (2024). Magneto-hydrodynamic mixed convection chemically rotating and radiating 3D hybrid nanofluid flow through porous media over a stretched surface. *Mathematical Modelling and Numerical Simulation with Applications*, 4(4), 495-513. <https://doi.org/10.53391/mmnsa.1438636>